Available online at www.sciencedirect.com
ScienceDirect
Energy Conversion and Management 49 (2008) 863–872
ENERGY CONVERSION & MANAGEMENT
www.elsevier.com/locate/enconman

# Performance evaluation of standing column well for potential application of ground source heat pump in Jordan

A. Al-Sarkhi, E. Abu-Nada, S. Nijmeh, B. Akash *

*Department of Mechanical Engineering, Hashemite University, Zarqa 13115, Jordan*

Received 12 April 2006; accepted 29 June 2007
Available online 20 August 2007

**Abstract**

Numerical simulation of the heat and fluid flows for the standing column well (SCW) and porous medium around the borehole of the ground source heat pump has been investigated. The finite difference technique was used. Parametric study for several variables has been developed. For example, different bleed ratios of 0.10, 0.20 and 0.30 and far-away temperatures ranging from 15 °C to 60 °C were investigated. An increase in bleed ratio and the far-away temperature will increase the outlet water temperature from the SCW, retuning back to the heat pump. The effect of porosity, ranging from 0.05 to 0.275, was also considered. Increasing porosity decreases the water outlet temperature. Similarly, the effects of Nusselt and Reynolds numbers in the ranges of 15–500 and 1000–11,000, respectively are reported in this paper. Nusselt and Reynolds numbers decrease with the water outlet temperature. The SCW can be employed as a good ground heat exchanger in a geothermal assisted heat pump system. A polynomial correlation of Nusselt number in terms of Reynolds number has been developed.


*Keywords:* Standing column well; Ground source heat pump; Jordan

## 1. Introduction

Jordan has proper geological and hydrological conditions to be considered as having a potential resource of geothermal energy. This potential may improve the overall performance of the ground source heat pump (GSHP) or geothermal heat pump (GHP), especially when using the standing column well (SCW). The expression GSHP refers to a heat pump system that uses either the ground or a water reservoir as a heat source or sink. Heat can be removed from the ground at comparatively low temperatures; the temperature is increased through the heat pump and is then used in a heating system during the cold season. For cooling in summer, the system can be reversed, and heat from the building can be rejected into the ground for greatly valuable space cooling. The ground system connects the heat pump to the underground and permits either removal of heat from the ground or rejection of heat into the underground. The GHP or GSHP is considered to be one of the world's fastest growing renewable energy applications [1,2]. They have an annual increase of about 10% in the USA and Europe. The reported number of installed units all over the world exceeds one million. The main advantage of the GHP is that it utilizes the ground temperature as a source of heat. Extensive research has been found in the literature on GSHP systems, particularly on the single U-tube ground heat exchanger [3–6] or in the general closed-loop GSHP [7]. Recently, some designs used horizontal closed loops for heating and cooling applications [8,9].

It was noted that the improved overall performance of the geothermal heat pump in the areas of proper geological and hydrological parameters is the reason for the latest increase in research work on the standing column well. Recently, the SCW received much attention because of its lower installation cost, lower running cost and improved

* Corresponding author. Tel.: +962 5 390 3333x4390; fax: +962 5 382 6613.
*E-mail address:* bakash@hu.edu.jo (B. Akash).

0196-8904/$ - see front matter © 2007 Elsevier Ltd. All rights reserved.
doi:10.1016/j.enconman.2007.06.028

**Nomenclature**

| | |
|---|---|
| bleed | mass fraction of bleed rate from total mass flow rate |
| $Cp_l$ | specific heat of water (J/kg K) |
| $Cp_s$ | specific heat of solid (J/kg K) |
| $D$ | borehole diameter (m) |
| $E$ | stretching parameter |
| $f$ | Moody friction factor |
| GSHP | ground source heat pump |
| GHP | geothermal heat pump |
| $h$ | convective heat transfer coefficient (W/m$^2$ K) |
| $h_{borehole}$ | convection heat transfer coefficient (W/m$^2$ K) |
| $k_{eff}$ | effective thermal conductivity for porous medium (W/m K) |
| $k_l$ | thermal conductivity of water (W/m K) |
| $k_s$ | thermal conductivity of solid (W/m K) |
| $L$ | borehole depth (m) |
| $m$ | total mass of water inside borehole (kg) |
| $\dot{m}$ | mass flow rate (kg/s) |
| $n$ | porosity of porous medium |
| $Nu$ | Nusselt number |
| $Pe$ | Peclet number ($Pe = Re\,Pr$) |
| $Pr$ | Prandtl number |
| SCW | standing column well |
| $V_r$ | radial average ground water velocity (m/s) |
| $V_{rb}$ | radial average ground water velocity at borehole surface (m/s) |
| $q$ | heat flux (W/m$^2$) |
| $r_b$ | borehole radius (m) |
| $r_i$ | radial distance at location $i$ (m) |
| $r_\infty$ | far-away radius (m) |
| $r$ | radius (m) |
| $R$ | thermal resistance (K/W) |
| $R_b$ | borehole thermal resistance (K/W) |
| $Re$ | Reynolds number |
| $Re_\varepsilon$ | roughness Reynolds number |
| $T_\infty$ | far-away temperature (°C) |
| $T_b$ | borehole surface temperature (°C) |
| $T_f$ | borehole average water temperature (°C) |
| $T_{f,out}$ | water temperature leaving well (°C) |
| $T_{f,in}$ | water temperature returning to well (°C) |
| $t$ | time (s) |
| $T_{fold}$ | temperature at previous time step (°C) |

*Greek symbols*

| | |
|---|---|
| $\alpha_s$ | soil thermal diffusivity |
| $\Delta t$ | time increment |
| $\rho_l$ | density of water |
| $\rho_s$ | density of solid |
| $\upsilon$ | kinematic viscosity of water |
| $\beta$ | $\rho_l Cp_l$ |
| $\xi$ | coordinate in computational domain |
| $\alpha_{thermal}$ | ratio $(k_{eff}/(\rho Cp)_{eff})$ |

*Subscripts*

| | |
|---|---|
| in | inlet |
| out | outlet |
| $\infty$ | far-away |
| b | borehole |
| f | fluid inside borehole |
| l | liquid (water) |
| s | solid (water saturated soil) |

*Superscripts*

| | |
|---|---|
| * | non-dimensional quantity |

overall performance of the GSHP in areas with suitable geological conditions such as Jordan. The SCW technology was evaluated and compared with other ground source heat pump systems [10]. The SCW system was found to have very important applications in commercial and industrial designs, since it requires shorter boreholes and gives more stable temperature, especially in regions of higher heating loads [11]. Most of the recent SCW designs are now focused on heat extraction [12]. Also, in another study, several assumptions regarding the transfer of heat between the different parts of the well were made [14]. The SCW system can be considered as a combination of a closed-loop coupled system and an open-loop ground water system. It operates by re-circulating water between the well and the heat pump as shown in Fig. 1. However, during peak temperature periods, it can "bleed" some water from the system to introduce groundwater flow into the well from the surrounding aquifer. One well may be sufficient, and more than one well connected in parallel can be used for higher loads. If the region has hard rock, deep bores are drilled, thereby constructing a standing column of water from the still water level down to the bottom of the bore. During periods of high heat extraction or

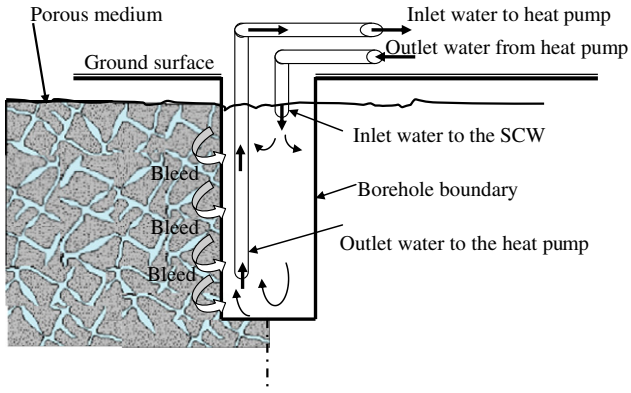


Fig. 1. Schematic diagram of the standing column well surrounded by porous medium.

rejection demand, if the well water temperature goes down too low or raises too high, standing column well systems can remove (bleed) part of the water out rather than returning it all to the well, which makes the water flow to the column from the surrounding aquifer to make up the flow. This reduces the column temperature during heat rejection in the hot seasons and heats the column during heat extraction in the cold seasons, thus bringing the well water temperature back to the normal operating condition and improving the system performance. Some studies were made on completely insulated wells. Others were made on the steady-state heat transfer between standing concentric well pipes and its surrounding to assist a heat pump [13]. A closed form analytical solution was derived for the concentric ground-coupled heat exchanger. An experimental investigation of the transient heat and mass transfer in a "thermal well" system was conducted [15]. Two wells were installed; one at 15 m depth and the other at 325 m to be used in a large commercial system with 70 kW cooling capacity. A derivation of a simplified mathematical model was performed to analyze the coupled thermo-hydraulic energy transfer by conduction and convection in an aquifer surrounding a thermal well [16]. The heat and ground water flows were assumed in the radial direction only. A research was conducted on the SCW using a submersible pump placed at the top of the borehole [17]. A two-dimensional model of a SCW was investigated numerically [10]. The model was used for a parametric study to investigate the effect of the most important design parameters on the well performance. Results showed that the groundwater percentage of bleed is the most important parameter for improving the well performance. This paper presents a model somewhat similar to the Rees et al. model [10], except it has the energy equation solved in dimensionless form in which a parametric study can be done easily and more efficiently. Our proposed model is a one-dimensional one, which is less computationally demanding than the two-dimensional Rees et al. [10] model. It uses a grid generator technique such that a fine grid at the wall of the borehole can be made (in significant places) and a course grid used in less significant regions. Most importantly, the parametric study focuses on parameters related to Jordan.

## 2. Geothermal energy resources in Jordan

Jordan has enormous underground energy resources in many parts of the country in the form of thermal underground hot water (wells and thermal springs). However, its main use is limited to therapeutic application and tourism. Jordan has a serious energy problem due to its complete dependence on imported oil, which makes a huge burden on its budget. Thermal springs form the main source of geothermal energy in Jordan, having a temperature range of 20 °C and up to 62 °C [18]. These springs are distributed along the eastern escarpment of the Jordan and Dead Sea graben (200 km). About 100 thermal wells drilled for water in the Dead Sea-Rift Valley, the Area of the Azraq Basin and Risha (Northeast Jordan) and the area south of Queen Alia Airport have low to intermediate water temperature. A summary of these thermal wells and springs was reported [19]. They are presented in Table 1.

The variation of underground temperature with depth ($x$) at any time ($t$), based on the average surface temperature ($T_a$) and soil properties, can be calculated from the following relationship [20]:

$$T = T_m - T_a \times \exp\left(-x\left(\frac{\pi}{365\alpha_s}\right)^{0.5}\right)\cos\left(\frac{2\pi}{365}\left(t - t_{cd} - \frac{x}{2}\left(\frac{\pi}{365\alpha_s}\right)^{0.5}\right)\right) \quad (1)$$

where $\alpha_s$ is soil thermal diffusivity, $T_m$ is the mean temperature, $T_a$ is temperature amplitude of air $= 1/2(T_{max} - T_{min})$ and $t_{cd}$ is the day of year when coldest air temperature occurs. Eq. (1) was applied to the location of Queen Alia International Airport in Amman, Jordan. The result is presented in Fig. 2, which shows the calculated underground temperature distribution for the months of January, April, July and October. For example, the temperature increases with depth for the month of January, while it decreases for the month of July. However, the temperature at a depth of about 30 m and deeper positions remains constant at about 16 °C throughout the year. This temperature is considered a good environmental source for both heating and cooling systems. On the other hand, the temperature distribution of the

Table 1
Thermal springs and wells in Jordan

| Thermal Spring location | Flowrate ($m^3/h$) | Temperature range (°C) |
|---|---|---|
| *Thermal springs* | | |
| Himmeh Thermal springs | 28 | 28–43 |
| Abu Thableh thermal spring | 17 | 37 |
| Deir Alla thermal spring | 17 | 35 |
| Wadi Hisban thermal Spring | – | 32 |
| Jerash thermal spring | 10 | 28 |
| Ain El Hammam | | 36 |
| El Dachruk (Zarqa river) C A in Suweimeh | | 34 |
| | | 27 |
| Ain Ez Zarqa | | 20–34 |
| Zarqa Ma'in (60 thermal springs) | | 63 |
| Burbeita | | 38 |
| Afra springs | 50–100 | 44–48 |
| Zara (45 thermal springs) | | 53 |
| Zara 1 | 800 | 54 |
| Zara 22 | 67 | 59 |
| Wadi Ibn Hammad springs | | 35 |
| Weida'a Thermal spring | | 32 |
| North Shauna well | 350 | 57 |
| Kafrain wells | | 33–36 |
| *Wells* | | |
| Zara and Zarqa main exploration wells | | |
| A – GTZ 2D | | 68.5 |
| B – GTZ 3D | | 57 |
| TSD1 well – Ghor El Haditha area | 400 | 50 |

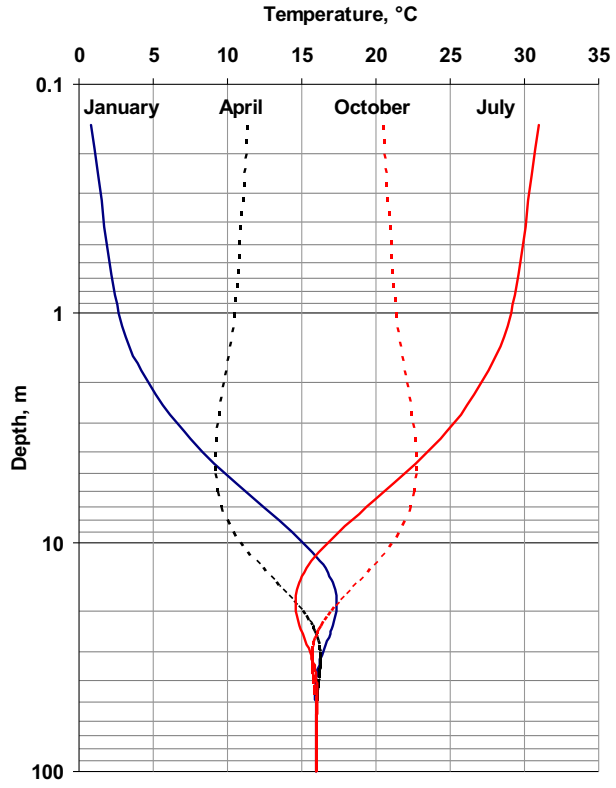


Fig. 2. Underground temperature distribution in the Queen Alia International Airport, Amman, Jordan.

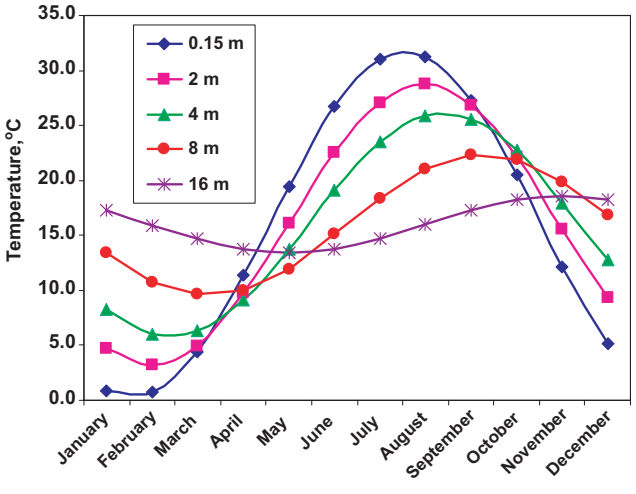


Fig. 3. The temperature distribution of the underground soil around the year for Queen Alia International Airport, Amman, Jordan.

underground soil around the year for the same location is presented in Fig. 3 for year round. Results from the model are consistent with those obtained experimentally [21]. The temperature fluctuation decreases with depth.

## 3. Standing column well

Standing column well systems will be one of the best choices in the areas of thermal springs and wells. The simulation of the one-dimensional model for the standing column well shown in Fig. 4 will be explained in the following section.

### 3.1. One-dimensional standing column well model

The computational time required to simulate directly two-dimensional or three-dimensional models is generally very expensive and tedious. Direct numerical simulation is unlikely to be used for the purpose of design and energy calculations. However, the present one-dimensional model is more practical with respect to the saving in computational time and memory requirement.

The present model uses similar equations to those in the model by Rees et al. [10] with the following modifications: the present method uses a one-dimensional finite difference method rather than the two-dimensional finite volume method in the Rees model; the governing equations in the present method have been transformed into a non-dimensional form, which allows non-dimensional parametric study to be done easily. Some simplification to the flow model also has been implemented in the present work to make the current model simpler and easier to use on one hand and faster in computation on the other hand.

The present model has the following assumptions:

- The porous medium is homogeneous and isotropic.
- The far-away temperature reaches a constant value (isothermal surface).
- Homogeneous flow of water (bleed) around a borehole surrounded by a porous medium as shown in Fig. 4.

The assumption of radial water flow (bleed) with no heat or water flow in the vertical direction is realistic if the well depth is much larger than the well diameter, which is the case in most applications. The computations in the one-dimensional model are done in two steps:

*First*: one-dimensional energy equation (advection–diffusion equation) for the porous medium surrounding the borehole is solved by the finite difference method. The temperature distribution from the far field ($T_\infty$) down to the borehole wall temperature is found.
*Second*: fluid in the borehole is treated as a whole mass of liquid. Then, an energy balance equation is used to find the temperature of the fluid going back to the heat pump.

### 3.2. Governing equations

The energy equation in the radial direction, $r$, with or without bleed, in the porous medium is written as:

$$\alpha\frac{\partial T}{\partial t}+\beta V_r\frac{\partial T}{\partial r}=\frac{1}{r}\frac{\partial}{\partial r}\left(k_{\text{eff}}r\frac{\partial T}{\partial r}\right) \tag{2}$$

where

$$\alpha=n\rho_l\text{Cp}_\text{l}+(1-n)\rho_\text{s}\text{Cp}_\text{s}=(\rho\text{Cp})_{\text{eff}} \tag{3}$$

$$\beta=\rho_l\text{Cp}_\text{l} \tag{4}$$

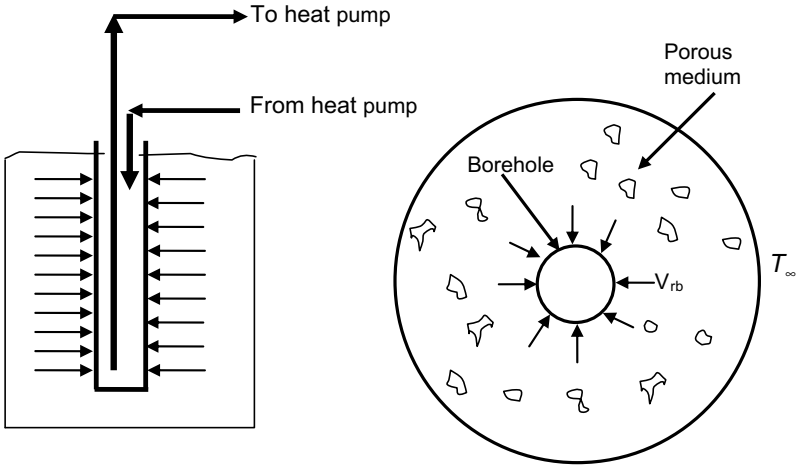


Fig. 4. One-dimensional model for the standing column well.

$$k_{\text{eff}} = nk_l + (1-n)k_s \tag{5}$$

$k_{\text{eff}}$ is the effective thermal conductivity (W/m K), $\rho_l$ is the density of the water (kg/m$^3$), $\rho_s$ is the density of the solid rock (kg/m$^3$), $Cp_l$ and $Cp_s$ are the specific heats of water and solid (J/kg K), respectively, and $n$ is the porosity.

By introducing the following dimensionless variables:

$$T^* = \frac{T}{T_\infty}; \qquad r^* = \frac{r}{r_b}; \qquad t^* = \frac{t}{(r_b/|V_{rb}|)} \tag{6}$$

where $T_\infty$ is the far-away temperature at the end of the computational domain, $r_b$ is the borehole radius and $V_{rb}$ is the radial average ground water velocity at the borehole surface.

By substituting the dimensionless variables into Eq. (2), and dropping the asterisks, Eq. (2) is rewritten as:

$$\frac{\partial T}{\partial t} + \frac{\beta}{\alpha} V_r \frac{\partial T}{\partial r} = \frac{k_{\text{eff}}}{r_b V_{rb} \alpha}\left[\frac{1}{r}\frac{\partial}{\partial r}\left(r\frac{\partial T}{\partial r}\right)\right] \tag{7}$$

but

$$\frac{k_{\text{eff}}}{r_b V_{rb}\alpha} = \frac{k_{\text{eff}}}{r_b V_{rb}(\rho Cp)_{\text{eff}}} = \frac{k_{\text{eff}}/(\rho Cp)_{\text{eff}}}{r_b V_{rb}} = \frac{\alpha_{\text{thermal}}}{r_b V_{rb}} = \frac{1}{Pe} \tag{8}$$

where

$$Pe = \frac{V_{rb} r_b}{\alpha_{\text{thermal}}} \tag{9}$$

$Pe$ is the Peclet number, $V_r$ is the average radial ground water velocity and $\alpha_{\text{thermal}}$ is the ratio $(k_{\text{eff}}/\rho \text{Cp})_{\text{eff}}$.

Then, the energy equation in the final (dimensionless) form becomes

$$\frac{\partial T}{\partial t} + \frac{\beta}{\alpha} V_r \frac{\partial T}{\partial r} = \frac{1}{Pe}\left[\frac{1}{r}\frac{\partial}{\partial r}\left(r\frac{\partial T}{\partial r}\right)\right] \tag{10}$$

$$\text{Let } C_r = \frac{\beta}{\alpha} \tag{11}$$

Then, the dimensionless form of the energy equation is as in Eq. (12)

$$\frac{\partial T}{\partial t} + C_r V_r \frac{\partial T}{\partial r} = \frac{1}{Pe}\left[\frac{1}{r}\frac{\partial}{\partial r}\left(r\frac{\partial T}{\partial r}\right)\right] \tag{12}$$

*3.2.1. Transformation of governing equation*

The following transformation transfers the non-dimensional physical domain in Fig. 5a into the computational domain shown in Fig. 5b.

Define $r = e^{\pi\xi}$ and substituting it in the governing equation given by Eq. (12) yields

$$\frac{\partial T}{\partial t} + \frac{C_r}{E} V_r \frac{\partial T}{\partial \xi} = \frac{1}{PeE^2}\frac{\partial^2 T}{\partial \xi^2} \tag{13}$$

where $E = \pi e^{\pi\xi}$ and $\xi$ is the coordinate in the computational domain.

*3.2.2. Ground water velocity*

The average ground water velocity ($V_{ri}$) at any radial distance, $r_i$, is determined from the continuity equation as:

$$V_{ri} = -\frac{1}{n}\frac{\dot{m} \times (\text{bleed})}{\rho 2\pi r_i L} \tag{14}$$

At the borehole

$$V_{rb} = -\frac{1}{n}\frac{\dot{m} \times (\text{bleed})}{\rho 2\pi r_b L} \tag{15}$$

where bleed is the mass fraction of bleed rate from the total flow rate, $\dot{m}$ is the mass flow rate, $L$ is the borehole depth and $\rho$ is the density of the liquid (water) in the borehole.

The bleed rate is always flowing into the borehole, so its sign is always negative.

Normalizing the radial ground water velocity by the borehole velocity yields

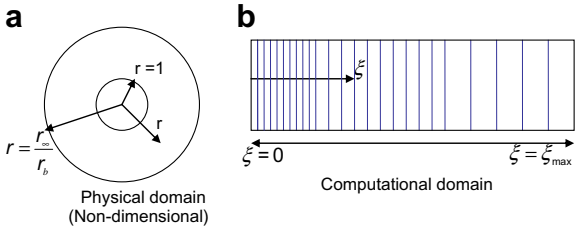


Fig. 5. Physical and transformed computational domain.

$$V_r^* = \frac{V_r}{V_{rb}} = \frac{r_b}{r_i} = \frac{1}{r^*} \tag{16}$$

Using the computational domain transformation yields

$$V_r^* = \frac{1}{r^*} = \frac{1}{e^{\pi\xi}} = \frac{\pi}{E} \tag{17}$$

Dropping the asterisks

$$V_r = \frac{\pi}{E} \tag{18}$$

### 3.3. Boundary conditions

The following boundary conditions are applied:

#### 3.3.1. Far-away boundary condition

$$\text{At } r = r_\infty, \rightarrow T = T_\infty \quad \text{(physical-dimensional domain)}$$
$$\text{At } r = \frac{r_\infty}{r_b}, \rightarrow T = 1 \quad \text{(physical non-dimensional domain)}$$
$$\text{At } \xi = \xi_{max}, \rightarrow T = 1 \quad \text{(computational domain)}$$

where $r_\infty$ is the far-away radius at the end of the domain and $T_\infty$ is the far-away temperature.

#### 3.3.2. Borehole boundary condition

A heat balance at the borehole states that the rate of heat transfer by conduction at the borehole wall equals the heat transferred by convection from the borehole to the fluid in the borehole, i.e.,

- Physical-dimensional domain:

$$\text{At } r = r_b, \rightarrow q = \frac{T_b - T_f}{R_b(2\pi r_b L)} \tag{19}$$

  where $T_b$ is the borehole surface temperature, $T_f$ is the borehole average temperature and $R_b$ is the borehole thermal resistance.

- Physical non-dimensional domain:

$$\text{At } r = 1, \rightarrow q = -k_{eff}\frac{T_\infty}{r_b}\frac{dT}{dr} = \frac{T_\infty(T_b - T_f)}{R_b}\frac{1}{2\pi r_b L} \tag{20}$$

- computational domain:

$$q = -k_{eff}\frac{T_\infty}{r_b E}\frac{dT}{d\xi} = \frac{T_\infty(T_b - T_f)}{R_b}\frac{1}{2\pi r_b L} \tag{21}$$

An under relaxation factor ($r_f$) was applied to the heat flux in the form

$$q = (1 - r_f)q_{old} + r_f q \tag{22}$$

where, $q_{old}$ is the heat flux in the previous iteration, $r_f$ is the under relaxation factor, $T_{f,in}$ is the water temperature returning to the well, $T_{f,out}$ is the water temperature leaving the well and $T_b$ is the borehole surface temperature.

The governing equations were solved by the fully implicit finite difference technique.

### 3.4. Output water temperature from the standing column well

Taking into consideration the groundwater coming to the borehole (the bleed rate), and making an energy balance on the water contained in the borehole, the average water temperature in the standing column well, $T_f$, can be written as:

$$T_f = \frac{(1 - \text{bleed})T_{f,in} + (\text{bleed})T_b + T_{f,out}}{2} \tag{23}$$

Using the above equation, the output temperature coming out of the SCW ($T_{f,out}$) is:

$$T_{f,out} = 2T_f - (1 - \text{bleed})T_{f,in} - (\text{bleed})T_b \tag{24}$$

Considering the energy balances over the control volume around the borehole shown in Fig. 6, the energy balance equation of the water in the borehole can be written as:

$$mCp\frac{dT_f}{dt} = \dot{m}(1 - \text{bleed})CpT_{f,in} + \dot{m}(\text{bleed})CpT_b - \dot{m}CpT_{f,out} + \frac{T_b - T_f}{R_b} \tag{25}$$

The bleed water from the surrounding porous medium enters the borehole at the borehole temperature $T_b$. Substituting for $T_{f,out}$ from Eq. (24) into Eq. (25) yields,

$$mCp\frac{dT_f}{dt} = 2\dot{m}(1 - \text{bleed})CpT_{f,in} + 2\dot{m}(\text{bleed})CpT_b - 2\dot{m}CpT_f + \frac{T_b - T_f}{R_b} \tag{26}$$

Using the non-dimensional parameters

$$T^* = \frac{T}{T_\infty}; \qquad t^* = \frac{t}{(r_b/|V_{rb}|)}$$

Using the forward difference technique to discretize the left hand side of Eq. (26) by letting $T_{f,old}$ be the known value of the average water temperature $T_f$ at time $t$, the quantity $T_f$ will be the unknown temperature at time $t + \Delta t$.

$$\frac{dT_f^*}{dt^*} = \frac{T_f^* - T_{f,old}}{\Delta t^*} \tag{27}$$

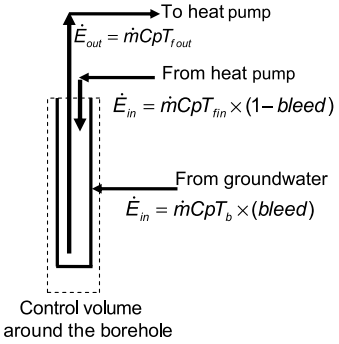


Fig. 6. The energy balance in the borehole model.

Table 2
The cases studied in this study

| Case # | $\dot{m}$ (kg/s) | Porosity (%) | Bleed (%) | $T_\infty$ (°C) | $R_\infty$ (m) | $T_{fin}$ (°C) | *Re* | *Nu* |
|---|---|---|---|---|---|---|---|---|
| 1 | 1.3 | 0.275 | 0.1 | 30 | 65 | 7 | 11035 | 486 |
| 2 | 1 | 0.275 | 0.1 | 30 | 65 | 7 | 8488 | 389 |
| 3 | 0.5 | 0.275 | 0.1 | 30 | 65 | 7 | 4244 | 207 |
| 4 | 0.2 | 0.275 | 0.1 | 30 | 65 | 7 | 1698 | 46 |
| 5 | 1.3 | 0.275 | 0.2 | 30 | 65 | 7 | 11035 | 486 |
| 6 | 1 | 0.275 | 0.2 | 30 | 65 | 7 | 8488 | 389 |
| 7 | 0.5 | 0.275 | 0.2 | 30 | 65 | 7 | 4244 | 206 |
| 8 | 0.2 | 0.275 | 0.2 | 30 | 65 | 7 | 1698 | 46 |
| 9 | 1 | 0.15 | 0.1 | 30 | 65 | 7 | 8488 | 389 |
| 10 | 1 | 0.1 | 0.1 | 30 | 65 | 7 | 8488 | 389 |
| 11 | 1 | 0.05 | 0.1 | 30 | 65 | 7 | 8488 | 389 |
| 12 | 1 | 0.05 | 0.1 | 20 | 65 | 7 | 8488 | 389 |
| 13 | 0.2 | 0.05 | 0.1 | 30 | 65 | 7 | 1698 | 46 |
| 14 | 0.2 | 0.05 | 0.1 | 20 | 65 | 7 | 1698 | 46 |
| 15 | 0.1387 | 0.1 | 0.1 | 30 | 65 | 7 | 1177 | 16 |
| 16 | 0.1387 | 0.275 | 0.1 | 30 | 65 | 7 | 1177 | 16 |
| 17 | 0.1387 | 0.05 | 0.1 | 30 | 65 | 7 | 1177 | 16 |
| 18 | 0.1387 | 0.15 | 0.1 | 30 | 65 | 7 | 1177 | 16 |
| 19 | 0.2 | 0.05 | 0.3 | 40 | 65 | 7 | 1698 | 45 |
| 20 | 0.2 | 0.05 | 0.2 | 40 | 65 | 7 | 1698 | 46 |
| 21 | 0.2 | 0.05 | 0.1 | 40 | 65 | 7 | 1698 | 46 |
| 22 | 0.2 | 0.05 | 0.01 | 40 | 65 | 7 | 1698 | 46 |
| 23 | 0.2 | 0.05 | 0.001 | 40 | 65 | 7 | 1698 | 46 |
| 24 | 0.5 | 0.05 | 0.01 | 40 | 65 | 7 | 4244 | 206 |
| 25 | 1 | 0.05 | 0.01 | 40 | 65 | 7 | 8488 | 389 |
| 26 | 0.2 | 0.05 | 0.01 | 50 | 65 | 7 | 1698 | 46 |
| 27 | 0.2 | 0.05 | 0.1 | 50 | 65 | 7 | 1698 | 45 |
| 28 | 0.5 | 0.05 | 0.01 | 50 | 65 | 7 | 4244 | 206 |
| 29 | 1 | 0.05 | 0.01 | 50 | 65 | 7 | 8488 | 388 |
| 30 | 1 | 0.05 | 0.1 | 50 | 65 | 7 | 8488 | 386 |
| 31 | 0.5 | 0.05 | 0.1 | 50 | 65 | 7 | 4244 | 204 |
| 32 | 0.5 | 0.05 | 0.1 | 40 | 65 | 7 | 4244 | 205 |
| 33 | 0.5 | 0.05 | 0.1 | 30 | 65 | 7 | 4244 | 206 |
| 34 | 0.5 | 0.05 | 0.1 | 20 | 65 | 7 | 4244 | 206 |
| 35 | 1 | 0.05 | 0.1 | 40 | 65 | 7 | 8488 | 387 |
| 36 | 0.2 | 0.275 | 0.3 | 30 | 65 | 7 | 1698 | 44 |
| 37 | 0.5 | 0.275 | 0.3 | 30 | 65 | 7 | 4244 | 201 |
| 38 | 1 | 0.275 | 0.3 | 30 | 65 | 7 | 8488 | 381 |
| 39 | 1.3 | 0.275 | 0.3 | 30 | 65 | 7 | 11035 | 470 |
| 40 | 0.5 | 0.05 | 0.3 | 40 | 65 | 7 | 1698 | 193 |
| 41 | 0.5 | 0.05 | 0.2 | 40 | 65 | 7 | 4244 | 196 |
| 42 | 0.5 | 0.05 | 0.1 | 40 | 65 | 7 | 4244 | 200 |
| 43 | 0.5 | 0.05 | 0.01 | 40 | 65 | 7 | 4244 | 203 |
| 44 | 0.5 | 0.05 | 0.007 | 40 | 65 | 7 | 4244 | 204 |
| 45 | 1 | 0.05 | 0.3 | 40 | 65 | 7 | 8488 | 364 |
| 46 | 1 | 0.05 | 0.2 | 40 | 65 | 7 | 8488 | 370 |
| 47 | 1 | 0.05 | 0.1 | 40 | 65 | 7 | 8488 | 378 |
| 48 | 1 | 0.05 | 0.01 | 40 | 65 | 7 | 8488 | 385 |
| 49 | 1 | 0.05 | 0.007 | 40 | 65 | 7 | 8488 | 386 |
| 50 | 0.5 | 0.05 | 0.1 | 40 | 65 | 7 | 4244 | 202 |
| 51 | 0.5 | 0.1 | 0.1 | 40 | 65 | 7 | 4244 | 203 |
| 52 | 0.5 | 0.15 | 0.1 | 40 | 65 | 7 | 4244 | 203 |
| 53 | 0.5 | 0.275 | 0.1 | 40 | 65 | 7 | 4244 | 204 |

$$T_f^* = \frac{\frac{r_b \Delta t^*}{V_{rb} m Cp}\left[2\dot{m}(1-\text{bleed})Cp T_{f,in}^* + 2\dot{m} r Cp T_b^* + \frac{T_b^*}{R_b}\right] + T_{f,old}^*}{\left[1 + \frac{2\dot{m}Cp(r_b)\Delta t^*}{V_{rb}(mCp)} + \frac{r_b \Delta t^*}{V_{rb}(mCp)R_b}\right]} \quad (28)$$

Using the average water temperature, $T_f$, calculated from Eq. (23), the water temperature leaving the well, $T_{f,out}$, can be obtained from Eq. (24).

### 3.5. Borehole resistance and convection heat transfer coefficient

The borehole thermal resistance can be calculated as

$$R_b = \frac{1}{2\pi r_b h_{borehole} L} \quad (29)$$

The convection heat transfer coefficient $h_{borehole}$ can be calculated as:

$$h_{\text{borehole}} = Nu\frac{k_{\text{water}}}{2r_b} \tag{30}$$

where $k_{\text{water}}$ is the thermal conductivity of water.

The local Nusselt Number ($Nu$) can be calculated as in Bhatti and Shah [22]

$$Nu = \frac{(f/2)(Re-1000)Pr}{1+(f/2)^{1/2}\left[(17.42-13.77Pr_t^{0.5})Re_\varepsilon^{0.2}Pr^{0.5}-8.48\right]} \tag{31}$$

$$Pr_t = \begin{cases} 1.01-0.09Pr^{0.36} & 1 \leqslant Pr \leqslant 145 \\ 1.01-1.11(\ln Pr) & 145 \leqslant Pr \leqslant 1800 \\ 0.99-0.29(\ln Pr)^{1/2} & 1800 \leqslant Pr \leqslant 12,500 \end{cases} \tag{32}$$

where

$$Re_\varepsilon = \frac{Re\sqrt{f/2}}{D/\varepsilon} \tag{33}$$

$$Re = \frac{\dot{m}(2r_b)}{\rho_{\text{water}}\pi r_b^2 \upsilon} \tag{34}$$

where, $f$ is the friction factor calculated using the Colebrook–White developed formula [23] for the range of $4\times10^3 < Re < 10^8$ as follows

$$f = \frac{0.25}{\left[\log_{10}\left(\frac{\varepsilon}{3.7(2r_b)}+\frac{5.74}{Re^{0.9}}\right)\right]^2} \tag{35}$$

Moreover, for the case of $R < 2300$, $f$ is calculated using $f = 64/Re$. Where $\varepsilon$ is the surface roughness of the borehole, and $Re$ and $Pr$ are the Reynolds and Prandtl numbers, respectively.

## 4. Results and discussion

Parametric studies for the model explained in the previous section of more than 50 cases have been investigated. A summary of the studied parameters is presented in Table 2. This study was performed during the heating mode; i.e., energy is extracted from the ground (winter case) under a steady-state condition. The constant parameters used in the present study are summarized in Table 3. Fig. 7 shows the steady-state point as a function of the time steps. In this simulation, 600,000 time steps was set for all runs.

Fig. 8 shows the variation of the outlet temperature with Reynolds number (mass flow rate) at different bleed ratios. The outlet temperature of the water going to the heat pump decreases with increasing mass flow rate. Fig. 9 shows the effect of the far-away temperature on the water outlet temperature from the SCW. The outlet temperature going to the heat pump increases with increasing isothermal far-away surface temperature, $T_\infty$. The gradient of the outlet temperature of the water increases with decreasing Reynolds number. Fig. 10 shows the effect of the bleed ratio on the outlet water temperature. The outlet water temperature increases as the ground water flow rate going to the borehole increases. During the high demand of heat rejection (cooling) or extraction (heating), if the temperature of the water inside the well changes (either up or down), then part of the water going to the standing column well bleeds. Then, this can make water flow to the well from the surrounding aquifer to compensate for the amount of flow in the system. This procedure heats the well (raises the temperature) during the heat extraction season (in winter) and cools the well during the heat rejection season (in summer). This technique will somehow bring the well water temperature to its normal operation conditions and improve the standing column well system performance. The removed water (bleed water) can be drained or changed to the home water consumption. Fig. 11 shows the variations of the

Table 3
Constant parameters used in the present study

| Parameter | Value |
|---|---|
| SCW length, $L$ | 320 m |
| Radius of the borehole, $r_b$ | 0.075 m |
| Surface roughness of the borehole, $\varepsilon$ | 0.0015 m |
| Density of water, $\rho_w$ | 1000 kg/m3 |
| Density of solid, $\rho_s$ | 2700 kg/m3 |
| Thermal conductivity of water, $K_w$ | 0.6 W/m °C |
| Thermal conductivity of solid, $K_s$ | 3 W/m °C |
| Heat capacity of water, $Cp_w$ | 4189 J/kg °C |
| Heat capacity of solid, $Cp_s$ | 1000 J/kg °C |

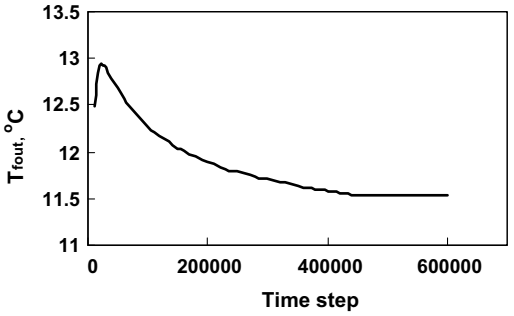


Fig. 7. Steady-state condition for water outlet temperature and time steps.

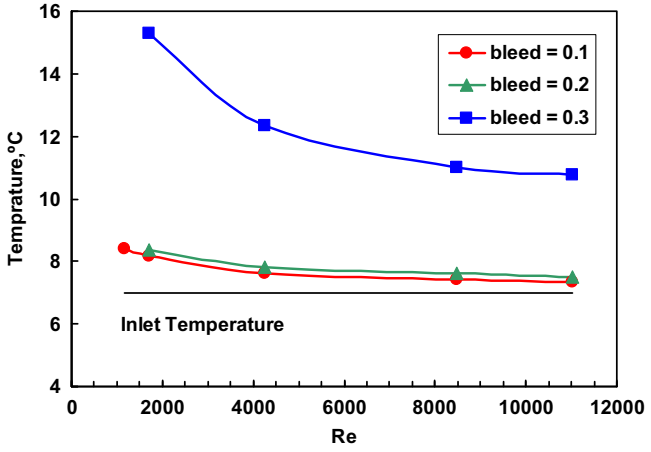


Fig. 8. Variation of the outlet temperature with Reynolds number.

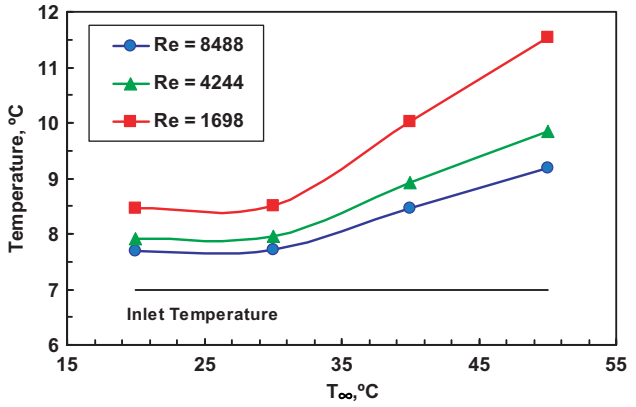


Fig. 9. Variation of the outlet temperature with the far-away temperature.

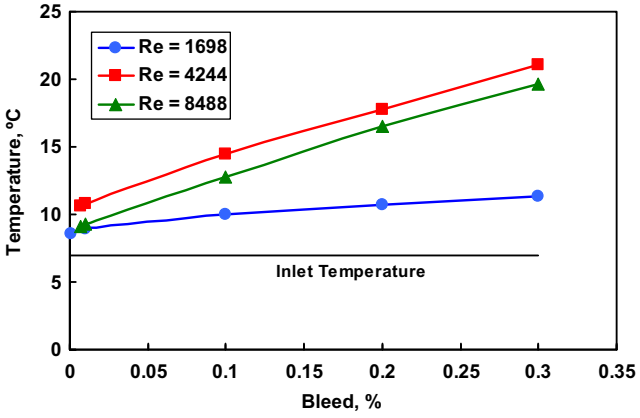


Fig. 10. Variation of the outlet temperature with the percentage of bleed.

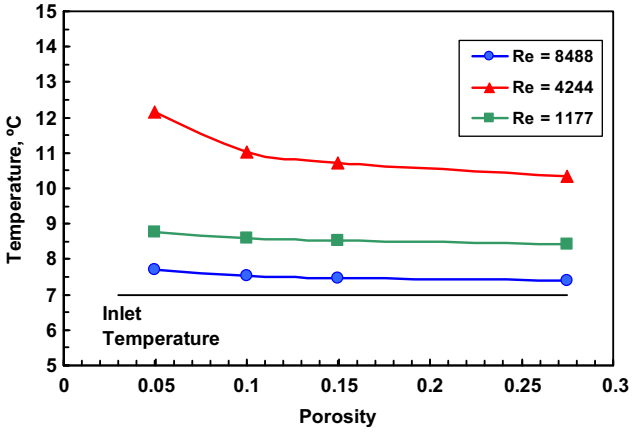


Fig. 11. Variation of the outlet temperature with the porosity.

outlet temperature from the SCW returning to the heat pump during the winter season (heating mode) with the porosity of the surrounding aquifer. As the porosity increases, the outlet temperature decreases slightly. Fig. 12 shows the effect of *Nu* on the outlet temperature of the water going out of the SCW to the heat pump. As *Nu* increases, the outlet temperature decreases, which is

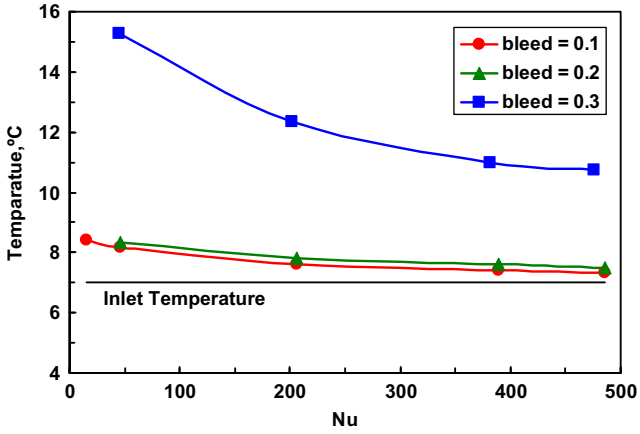


Fig. 12. Effect of Nusselt number on the outlet water temperature.

the same trend as for the Reynolds number versus the outlet water temperature. Fig. 13 shows the relation between the Reynolds and Nusselt numbers. The Nusselt number increases with Reynolds number according to the relationship that can be correlated by a polynomial of the third degree as follows:

$$Nu = 2 \times 10^{-10} Re^3 - 5 \times 10^{-6} Re^2 + 8.61 \times 10^{-2} Re - 81.984 \quad (36)$$

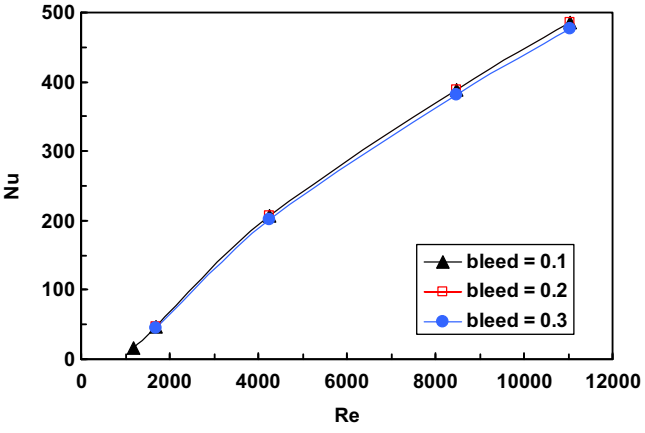


Fig. 13. Variation of the Reynolds number with Nusselt number.

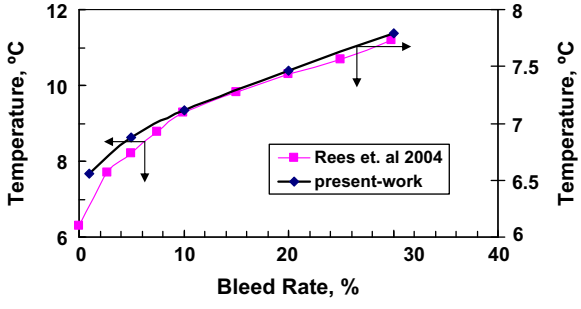


Fig. 14. The effect of bleed rate on the water outlet temperature for the present work and [10].

Fig. 14 shows a comparison between the results obtained from the current study and those by Rees et. al. [10]. Both studies show that the outlet water temperatures versus the bleed rates have similar trends. The outlet temperature increases non-linearly with increasing bleed rate.

## 5. Conclusions

A one-dimensional parametric study for the performance of the standing column well has been performed numerically using a finite difference method. The heating mode (cold seasons) study was simulated. The effects of Reynolds number (mass flow rate), far-away isothermal temperature, bleed ratio and porosity of the surrounding porous medium have been investigated under steady-state conditions. The bleed ratio and the far away temperature increase the outlet water temperature from the SCW going back to the heat pump. Increasing porosity and the Nusselt and Reynolds numbers decrease the outlet water temperature.

Comparison of the current proposed model with another published model was performed and showed similar trends regarding the SCW outlet temperature relation as a function of bleed rate. The outlet temperature increases non-linearly with increasing bleed rate.

## Acknowledgements

The authors acknowledge the Abdul Hameed Shoman Fund for Supporting Scientific Research, Amman, Jordan, for their financial support through the project entitled "Modeling of Geothermal Energy Processes for Future Application in Jordan". Support by the Hashemite University is also acknowledged.

## References

[1] Lund J, Freeston D. World-wide direct uses of geothermal energy 2000. Geothermics 2001;30:29–68.
[2] Lund J, Sanner B, Rybach L, Curtis R, Hellstörm. Geothermal (ground-source) heat pumps: a world review. Geo-Heat Center Bulletin 2004;25(3):1–10.
[3] Deerman JD, Kavanaugh SP. Simulation of vertical U-tube ground-coupled heat pump systems using cylindrical heat source solution. ASHRAE Trans 1991;97(1):287–95.
[4] Gu Y, O'Neal D. Development of an equivalent diameter expression for vertical U-tubes used in ground-coupled heat pumps. ASHRAE Trans 1998;104(2):347–55.
[5] Yavuzturk C, Spitler JD. Comparative study to investigate operating and control strategies for hybrid ground source heat pump systems using a short time step simulation model. ASHRAE Trans 2000;106(2):192–209.
[6] Yavuzturk C, Spitler J, Rees S. A transient two-dimensional finite volume model for the simulation of vertical U-tube ground heat exchangers. ASHRAE Trans 1999;105(2):465–74.
[7] Chiasson AD, Spitler JD, Rees SJ, Smith MD. A model for simulating the performance of a shallow pond as s supplemental heat rejecter with closed-loop ground-source heat pump systems. ASHRAE Trans 2000;106(2):107–21.
[8] Inalli M, Esen H. Experimental thermal performance evaluation of a horizontal ground-source heat pump system. Appl Therm Eng 2004;24:2219–32.
[9] Inalli M, Esen H. Seasonal cooling performance of a ground-coupled heat pump system in a hot and arid climate. Renew Energ 2005;30:1411–24.
[10] Rees SJ, Spitler JD, Deng Z, Orio CD, Johnson CNA. study of geothermal heat pump and standing column well performance. ASHRAE Trans 2004;110(1):3–13.
[11] Sanner B. Shallow geothermal energy. Geo-Heat Center Bulletin 2001;22(3):19–25.
[12] Esen H, Inalli M, Esen M. Technoeconomic appraisal of a ground source heat pump system for a heating season in eastern Turkey. Energ Convers Manage 2006;47:1281–97.
[13] Oliver J, Braud H. Thermal exchange to earth with concentric well pipes. ASHRAE Trans 1981;24(4):906–10.
[14] Braud H, Klimkowki H, Oliver J. Earth source heat exchanger for heat pumps. ASHRAE Trans 1983;26:1818–22.
[15] Mikler V. A theoretical and experimental study of the "energy well" performance. Masters thesis, Pennsylvania State University, College Park, PA; 1993.
[16] Yuill GK, Mikler V. Analysis of the effect of induced groundwater flow on heat transfer from a vertical open-hole concentric-tube thermal well. ASHRAE Trans 1995;101(1):173–85.
[17] Orio CD. Geothermal heat pump applications industrial/commercial. Energ Eng 1999;96(3):58–66.
[18] Swarieh A. Geothermal energy resources in Jordan, country update. In: Proceedings world geothermal congress, Kyushu-Tokyo, Japan; 2000. p. 469–74.
[19] Sunna' B. Recommended approaches to develop the direct utilization of geothermal energy (hot water). In: Jordan int water demand management conference, Dead Sea, Jordan; 2004.
[20] Doherty PS, Al-Huthaili S, Riffat SB, Abodahab N. Ground source heat pump-description and preliminary results of Eco House system. Appl Therm Eng 24:2627–41.
[21] Nassar Y, El Noaman A, Abutaima A, Yousif S, Salem A. Evaluation of the underground soil thermal storage properties in Libya. Renew Energ 2006;31:593–8.
[22] Bhatti MS, Shah RK. In: Kakac S, Shah RK, Aung W, editors. Handbook of single-phase convective heat transfer. NY: Wiley; 1987.
[23] Streeter VL, editorHandbook of fluid dynamics. New York: McGraw-Hill; 1961.